Article

A Novel Coupler of Capacitive Power Transfer for Enhancing Underwater Power Transfer Characteristics

Xueqiang Zhang [1] and Jing Lian [1,2,*]

1　School of Automation, Nanjing University of Information Science and Technology, Nanjing 210044, China; 202213360033@nuist.edu.cn
2　Jiangsu Provincial Key Laboratory of Smart Grid Technology and Equipment, Southeast University, Nanjing 210096, China
*　Correspondence: 003594@nuist.edu.cn; Tel.: +86-19121928396

Abstract: Compared to inductive power transfer (IPT) technology, capacitive power transfer (CPT) technology offers unique advantages such as being cost-effective, lightweight, and free from eddy-current losses, making it more suitable for underwater power transfer. Unlike air, water can conduct electricity and the electric conductivity of different kinds of waters varies with different ion concentrations, which would greatly affect the equivalent model of the underwater couplers. To address this issue, multiple types of underwater coupler working in different kinds of water are compared and analyzed. The influence of the electrical conductivity of water on the capacitive coupler is comprehensively analyzed, and the novel capacitive coupler and its equivalent model are proposed to improve power transfer efficiency. To verify the theoretical analysis, the double-sided LC-compensated CPT circuit is built and tap water is used in the experiment. The experimental results are consistent with the theoretical analysis. In addition, the experimental results also validate the superiority of the proposed capacitive coupler compared to existing research.

Keywords: underwater; capacitive power transfer; capacitive coupler; double-sided LC compensation circuit

1. Introduction

In recent years, the fields of underwater resource exploration and deep-sea research have witnessed significant advancements, leading to a flourishing development of underwater equipment [1,2]. However, the issue of charging has emerged as a constraining factor impeding the progress of underwater equipment development [3]. The utilization of underwater wireless power transfer (WPT) technology holds promising potential in surmounting this bottleneck [4–6].

Inductive power transfer (IPT) and capacitive power transfer (CPT) are two main ways to realize WPT. IPT utilizes expensive Litz wire and magnetic cores to generate a high-frequency magnetic field for power transmission. A high-frequency magnetic field would induce an eddy current in a conductor. Consequently, commonly used IPT systems face challenges such as underwater eddy current losses [7,8]. A high-frequency electric field, rather than a magnetic field, is generated by metal plates in CPT. Compared to IPT, CPT possesses the advantages of having no eddy current loss, and being cheap and light. Therefore, it is important to conduct research on capacitive power transfer (CPT) in order to ascertain its viability for underwater applications [9]. The field of CPT has also seen extensive research efforts, leading to numerous research findings such as electric vehicles [10–12], underwater vehicles [13–15], and electric ship charging [3,16].

The typical CPT converters are composed of an input DC/AC inverter, a compensation circuit, a coupler, an output AC/DC rectifier, and a load [17]. The CPT coupler is often composed of four metal plates, with two metal plates placed on the primary side as power transmission plates and the other two metal plates placed on the secondary side as power

receiving plates. These metal plates are used to generate a high-frequency electric field for wireless power transmission [18]. Air is the most common dielectric material between the metal plates in CPT couplers [19]. However, in underwater environments, water serves as the medium between the metal plates; unlike other insulating materials, water exhibits some degree of electrical conductivity. Various types of water media display substantial differences in terms of electrical conductivity. Distilled water has minimal impurities and is essentially non-conductive, with a conductivity of 1.0 to 10.0 µS/cm [20]. Natural freshwater contains more conductive ions and impurities, with a conductivity of approximately 125 to 1250 µS/cm, while mineralized water has a conductivity of around 500 to 1000 µS/cm [21]. Seawater has a high concentration of conductive ions and impurities, with a conductivity of 30,000 µS/cm or higher [22].

When a CPT coupler is energized, if the dielectric between the plates is insulating, an electric field is induced between the plates. However, if the medium between the plates is conductive, a current is generated between the plates. Due to the inherent electrical conductivity of most natural water media, the equivalent model and operating principles of underwater CPT couplers differ significantly from those in air [23], rendering the coupler structures, equivalent models, and operating principles suitable for insulating media potentially inappropriate for underwater applications. Furthermore, differences in electrical conductivity between air and water would also alter the input and output characteristics of CPT systems.

To date, extensive research has been conducted on underwater CPT, yielding remarkable advancements in this field. Relative parameters are provided in Table 1. Researchers [24] have discovered that underwater CPT couplers exhibit a significant increase in equivalent capacitance when compared to an air medium. However, the power transmission level and energy transfer efficiency of underwater CPT systems consistently remain at a relatively low level. To enhance the power transmission efficiency of underwater CPT systems, an asymmetric coupler structure was proposed in [25] which reduced the area of one pair of metal plates. This increased the gap between the main capacitance and cross capacitance, improving the equivalent mutual capacitance. However, it is worth mentioning that the work utilized a comparatively low water medium conductivity of merely 2 µS/cm, which is significantly lower than natural water [20–22] and limits its applicability. In reference [26], a double-layer capacitive coupler was constructed under seawater, demonstrating an electrical energy transmission efficiency of 55.3% at a frequency of 308 Hz. However, it was noted that as the operating frequency increased, the formation of the double-layer capacitance became challenging. Therefore, double-layer capacitive couplers are primarily suitable for underwater CPT systems with very low operating frequencies. In reference [27], one pair of metal plates is insulated while the other pair remains uninsulated. However, reference [27] exhibits the lowest power transmission level and efficiency. And both [4,27] operate at frequencies ranging from tens to hundreds of MHz, resulting in extremely high design costs and difficulties during actual operation.

Table 1. The coupler structure, transmission power, and transmission efficiency of the existing underwater CPT system.

Reference	Insulation	Water Types	Transfer Distance	Input Power	Efficiency
[25]	All four aluminum plates are insulated	2 µS/cm	500 mm	365 W	60.17% (R = 37.5 Ω)
[26]	All four metal plates are uninsulated	Seawater	5 mm	\	55.3% (f = 308 Hz)
[27]	Only one pair of plates is insulated	Tap water	5 mm	51.8 mW	62.4% (R = 3 kΩ)
[28]	All four metal plates are uninsulated	Tap water	20 mm	\	85.1% (f = 33.3 MHz) 80.9% (f = 25.7 MHz)
[4]	All four metal plates are uninsulated	Freshwater	20 mm	400 W	90% (f = 107.7 MHz)

Based on the above analysis, the existing research has some limitations, such as a relatively higher frequency and lower electrical conductivity. In addition, in [4,26–28], only a small amount of water is added between the metal plates of the CPT coupler. Clearly, when the metal plates are fully immersed in a larger water tank, the system's efficiency will significantly decrease. To improve the power transfer efficiency of the underwater CPT system and broaden its range of applications, this paper proposes a novel capacitive coupler, which is shown in Figure 6 in Section 4. After a comprehensive comparison and analysis of multiple types of underwater coupler operating in diverse water environments, the equivalent model of the proposed coupler is built as shown in Figures 7 and 9 in Section 4. Additionally, the underwater double-sided LC-compensated CPT prototype based on the novel coupler is built as shown in Figure 10 in Section 4. Through experimental validation, it is demonstrated that the proposed novel underwater coupler can enhance the operational performance of CPT supply systems and powered devices in different media, thereby expanding the applicability of CPT.

The following is the organization of this paper. Section 2 shows the theoretical analysis and simulation of a single pair of metal plates, highlighting that when the medium is dielectric, the equivalent capacitance of underwater single pairs of metal plates significantly increases. Section 3 shows the theoretical analysis and simulation of two pairs of metal plates, indicating that when the medium is conductive, the equivalent mutual capacitance of underwater CPT couplers approaches zero, limiting power transmission. Additionally, the six equivalent capacitors formed by the four metal plates of the coupler mutually influence each other. Section 4 focuses on the design of the novel underwater CPT coupler structure and an analysis of its transmission characteristics. Section 5 presents the experimental validation and Section 6 provides the conclusions.

2. Research on a Single Pair of Metal Plates Submerged in Water

2.1. Theoretical Analysis of Equivalent Capacitance for the Single Pair of Metal Plates

Common underwater CPT couplers typically consist of two pairs of metal plates and insulating layers. Insulating layers are used to isolate the metal plates from the water medium. Before delving into the study of underwater CPT systems, a single pair of metal plates was first studied. The schematic diagram of a single pair metal plates in water medium is shown in Figure 1, where the orange parts represent the metal plates, the green parts represent the insulating layer, and the blue parts represent the water medium. Depending on the conductivity, the water medium can be considered either a non-conductive dielectric or a conductive conductor.
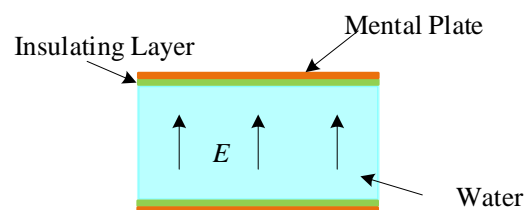

Figure 1. The structure of a single pair of metal plates in water medium.

When the water medium acts as a dielectric, the single pair of metal plates illustrated in Figure 1 can be equivalent to the structure shown in Figure 2, where C_{mica} represents the capacitance equivalently formed by a single insulating layer, while C_{water} represents the capacitance equivalently formed by the water medium. The formulas for calculating the capacitances C_{mica} and C_{water} are as follows:

$$C_{mica} = \frac{A\varepsilon_0\varepsilon_{r(mica)}}{d_1}, C_{water} = \frac{A\varepsilon_0\varepsilon_{r(water)}}{d_2}. \tag{1}$$

where A represents the surface area of the metal plates, d_1 is the thickness of the insulating layer, d_2 is the thickness of water, ε_0 is the vacuum's dielectric constant, $\varepsilon_{r(mica)}$ is the

insulation layer's relative dielectric constant, and $\varepsilon_{r(water)}$ is the water medium's relative dielectric constant. In this way, the equivalent capacitance C_{eq1} for a single pair of metal plates in water medium could be calculated as

$$C_{eq1} = \frac{1}{\frac{2}{C_{mica}} + \frac{1}{C_{water}}}. \tag{2}$$
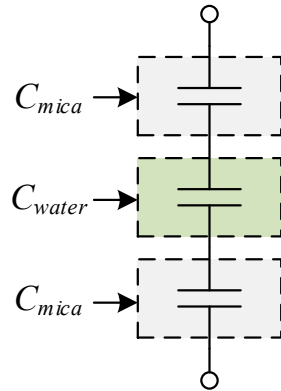

Figure 2. Equivalent capacitances of Figure 1.

When the water medium behaves as a conductor, current is generated between the plates. Consequently, high-frequency electric fields cannot exist within the conductor. Consequently, the equivalent capacitance C_{water} shown in Figure 2 cannot be formed. In this scenario, the equivalent capacitance C_{eq2} of the underwater single pair of metal plates is only related to C_{mica} and C_{mica}, where

$$C_{eq2} = \frac{1}{\frac{1}{C_{mica}} + \frac{1}{C_{mica}}}. \tag{3}$$

According to (1) and (3), when the water medium behaves as a conductor, the equivalent capacitance of the underwater single pair of metal plates is influenced by d_1, $\varepsilon_{r(mica)}$, and A. It is not dependent on the power transfer distance d_2 (i.e., the thickness of water) and the relative dielectric constant of the water medium $\varepsilon_{r(water)}$.

2.2. Simulation Analysis of the Equivalent Capacitance for a Single Pair of Metal Plates

To validate the accuracy of the theoretical analysis above, this section utilizes Maxwell 16.0 for analysis. A simulation model is constructed based on the structure shown in Figure 1, with aluminum chosen as the material for the metal plates and mica chosen as the material for the insulating layer. The relative dielectric constant of mica $\varepsilon_{r(mica)}$ is set to 5.7 and the relative dielectric constant of the water medium $\varepsilon_{r(water)}$ is set to 81. The dimensions of the metal plates are designed to be 200 mm $\times$ 200 mm $\times$ 2 mm, the thickness of the insulating layer d_1 is 4 mm, and the wireless power transmission distance d_2 is 4 cm. When the water medium acts as a dielectric, according to (1), the theoretical equivalent capacitances of the insulating layer and water are calculated as follows: C_{mica} = 504.5 pF and C_{water} = 716.9 pF. According to (2), the theoretical equivalent capacitance of the single pair of metal plates C_{eq1} is calculated as 186.6 pF. When the water medium behaves as a conductor, according to (3), the theoretical equivalent capacitance of the single pair of metal plates C_{eq2} is calculated as 252.25 pF.

To investigate the relationship between the water conductivity and the equivalent capacitance of a single pair of metal plates C_{eq}, different conductivities of water are tested, including 2 µS/cm, 100 µS/cm, 20,000 µS/cm, and 40,000 µS/cm. When the water conductivity is 2 µS/cm or 100 µS/cm, the water behaves as a dielectric, and when the water conductivity is 20,000 µS/cm or 40,000 µS/cm, the water behaves as a conductor.

In addition, the water is replaced by air as a reference. Specific simulation results are shown in Table 2.

Table 2. Equivalent capacitances of a single pair of metal plates in different media.

Conductivity	2 μS/cm	100 μS/cm	20,000 μS/cm	40,000 μS/cm	Air
Equivalent capacitance	188.32 pF	188.32 pF	254.8 pF	254.8 pF	9.43 pF

According to Table 2, when the conductivity of the water medium is 2 μS/cm or 100 μS/cm, the equivalent capacitance is approximately equal to the theoretical equivalent capacitance C_{eq1} where C_{eq1} = 186.6 pF. In this case, the water behaves as a dielectric and the equivalent capacitance is essentially unaffected by variations in the water conductivity. Similarly, when the water conductivity is 20,000 μS/cm or 40,000 μS/cm, the equivalent capacitance is approximately equal to the theoretical equivalent capacitance C_{eq2} where C_{eq2} = 252.25 pF. In this case, the water behaves as a conductor and variations in the water conductivity do not affect the equivalent capacitance of a single pair of metal plates submerged in water. The simulation results validate the theoretical analysis.

According to Table 2, it is evident that the equivalent capacitance significantly increased compared to the air medium, regardless of whether the water medium acts as a dielectric or a conductor. When water acts as a dielectric, its relative dielectric constant is approximately 81 times that of air. As a result, according to (2), the equivalent capacitance of a single pair of metal plates experiences a significant improvement. When water behaves as a conductor, the equivalent capacitance of a single pair of metal plates is independent of the power transmission distance but is inversely proportional to the thickness and relative dielectric constant of the insulating layer. Since the insulating layer is relatively thin and its relative dielectric constant is greater than that of air, according to (3), the equivalent capacitance of the single pair of metal plates also undergoes a significant improvement in this scenario.

In order to investigate the anti-misalignment performance of a single pair of metal plates, this section conducts Maxwell simulations using the coupler depicted in Figure 3. The dimensions of the metal plates are 200 mm × 200 mm × 2 mm, the thickness of the insulating layer d_1 is 4 mm, the distance for wireless power transmission d_2 is 4 cm, and the distance of misalignment x_{mis} is 10 cm. Specific simulation results are shown in Table 3.
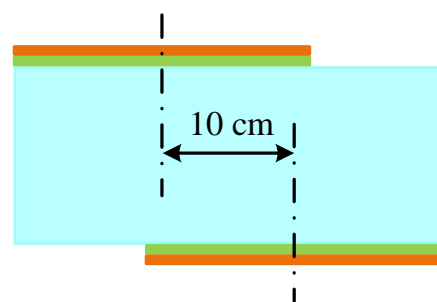

Figure 3. The structure of a single pair of metal plates in water medium with misalignment.

Table 3. Simulation values of equivalent capacitances of a single pair of metal plates in different media with misalignment.

Conductivity	2 μS/cm	100 μS/cm	20,000 μS/cm	40,000 μS/cm	Air Dielectric
Equivalent capacitance	131.09 pF	131.09 pF	256 pF	256 pF	7.07 pF

Based on the simulation data from Table 3, when the water conductivity is 2 μS/cm, the equivalent capacitance of a single pair of metal plates is equal to that when the water conductivity is 100 μS/cm. However, compared to Table 2, when the water conductivity

is 2 μS/cm or 100 μS/cm, the equivalent capacitances vary with coupler misalignment. Similarly, when the water conductivity is 20,000 μS/cm, the equivalent capacitance of a single pair of metal plates is equal to that when the water conductivity is 40,000 μS/cm. However, comparing this with the simulation data in Table 2 reveals that for these two conductivity values, the equivalent capacitance remains largely unchanged even when misalignment occurs. Therefore, when water acts as a conductor, the equivalent capacitance of a single pair of metal plates is essentially unaffected by misalignment. The equivalent capacitance is only influenced by the relative dielectric constant and thickness of the insulating material, as well as the surface area of the metal plates.

3. Research on Underwater CPT Couplers

The typical structure of an underwater CPT coupler is shown in Figure 4. Insulating layers separate metal plates from the water. For the CPT coupler depicted in Figure 4, any two metal plates can form an equivalent capacitance, resulting in six equivalent capacitances, C_{12}, C_{13}, C_{14}, C_{23}, C_{24}, and C_{34}, where the main capacitances are C_{13} and C_{24}, the cross capacitances are C_{14} and C_{23}, and the leakage capacitances are C_{12} and C_{34}. The corresponding equivalent circuit to Figure 4 is shown in Figure 5. Furthermore, the relationship between the equivalent mutual capacitance C_M and the six capacitance values mentioned above can be calculated as:

$$C_M = \frac{C_{24}C_{13} - C_{14}C_{23}}{C_{13} + C_{14} + C_{23} + C_{24}}. \tag{4}$$
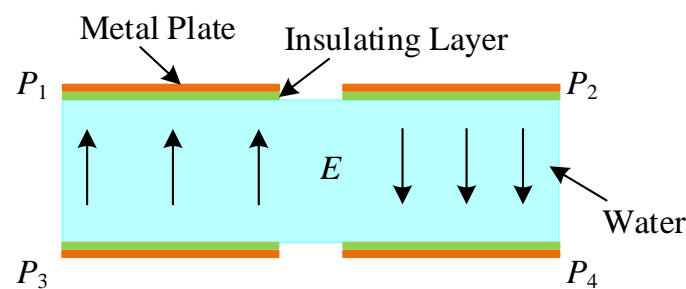

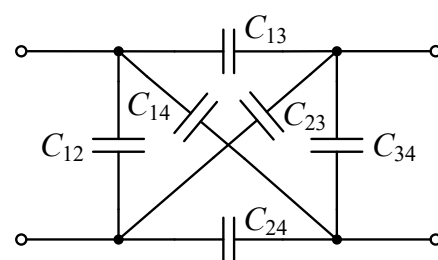**Figure 4.** The structure of a symmetrical underwater CPT coupler.

Figure 5. The equivalent circuit of a symmetrical underwater CPT coupler.

As mentioned in Section 2, when water behaves as a conductor, the equivalent capacitance of a single pair of metal plates under water is independent of misalignment. Therefore, it can be assumed that C_{13} formed by P_1 and P_3 is approximately equal to C_{14} formed by P_1 and P_4. According to (4), in this scenario, the equivalent mutual capacitance C_M of the underwater CPT coupler is approximately zero, making it challenging for electrical energy transmission.

To verify the above analysis, simulations are conducted using Maxwell simulation software based on the structure shown in Figure 4. The dimensions of the metal plates are 200 mm × 200 mm × 2 mm. The insulating material is mica. The thickness of a single mica layer d_1 is 4 mm. The power transmission distance d_2 is 4 cm. The distance

between P_1 and P_2 or P_3 and P_4 is set to 1 cm. The relative dielectric constant of mica $\varepsilon_{r(mica)}$ is 5.7, and the relative dielectric constant of the water $\varepsilon_{r(water)}$ is 81. Specific simulation results are shown in Table 4, where the main capacitance $C_{13} = C_{24}$, the cross capacitance $C_{14} = C_{23}$, and the leakage capacitance $C_{12} = C_{34}$. Furthermore, in order to facilitate a more accurate comparison, simulations are also conducted by replacing water with air in the simulation model.

Table 4. Equivalent capacitances of CPT couplers in different media.

Conductivity	2 μS/cm	100 μS/cm	20,000 μS/cm	40,000 μS/cm	Air Dielectric
Main capacitance	172.5 pF	172.5 pF	128.2 pF	128.1 pF	9.7 pF
Cross capacitance	17.6 pF	17.6 pF	128.2 pF	128.2 pF	0.43 pF
Leakage capacitance	20.4 pF	20.4 pF	129.0 pF	128.7 pF	2.4 pF
Mutual capacitance	77.45 pF	77.45 pF	0	0	4.62 pF

When the water conductivity is 2 μS/cm or 100 μS/cm, the water acts as a dielectric. Due to the relative dielectric constant of water being 81, compared to air, the mutual capacitance C_M experiences a significant increase, as indicated in Table 4. When the water conductivity is 20,000 μS/cm or 40,000 μS/cm, the mutual capacitance C_M is approximately zero. In this scenario, the transmission of electrical energy becomes challenging. The simulation analysis aligns with the theoretical analysis.

As water in the natural world possesses some level of conductivity, achieving high-performance electrical energy transmission in underwater CPT systems requires an increase in the mutual capacitance C_M. This can be achieved by widening the gap between the main capacitance and the cross capacitance according to (4). As analyzed in Section 2, the main capacitances and cross capacitances are only determined by the thickness and relative dielectric constant of the insulating material, along with the surface area of the metal plates. To achieve an improvement in C_M, the gap between the main capacitances and the cross capacitances of the underwater CPT coupler should be enlarged.

4. Analysis of an Underwater CPT System Based on a Novel Coupler

4.1. Design of a Novel Underwater CPT Coupler

Based on the analysis above, when water is dielectric, the equivalent mutual capacitance C_M significantly increases. However, when water is conductive, the equivalent mutual capacitance C_M approaches zero, making electrical energy transmission challenging. Natural water found in the environment contains impurities and ions, exhibiting varying degrees of electrical conductivity. Compared to good conductors like copper and silver, natural water has relatively high electrical resistivity. As a result, the equivalent resistance of underwater couplers cannot be ignored, and significant electrical losses will occur, thereby affecting the overall performance of underwater CPT systems. Since the equivalent mutual capacitance C_M of traditional underwater CPT couplers approaches zero, a novel CPT coupler with higher power transmission levels and efficiency should be proposed.

The novel underwater CPT coupler proposed in this paper is shown in Figure 6. In this design, the metal plates are made of aluminum, and the dimensions of metal plates P_a and P_c are set to 200 mm × 200 mm × 2 mm. To reduce the size of the coupler, metal plates P_b and P_d have dimensions of 100 mm × 100 mm × 2 mm. To enhance the equivalent mutual capacitance C_M of the underwater CPT coupler, insulating material is applied to isolate P_a and P_c from the water. Metal plates P_b and P_d are in direct contact with the water without insulation on their surfaces.

The equivalent circuit of the proposed CPT coupler is shown in Figure 7. Each branch of the circuit is modeled as a combination of equivalent capacitance and equivalent conductance. The components C_{ac}, C_{ab}, C_{cd}, C_{bc}, and C_{ad} represent the equivalent capacitances formed by the coupling of metal plates P_a and P_c, P_a and P_b, P_c and P_d, P_b and P_c, and P_a and P_d, respectively. To measure the losses in the coupler, G_{ac}, G_{ab}, G_{ad}, G_{cd}, G_{bc}, and G_{bd} represent equivalent conductances.
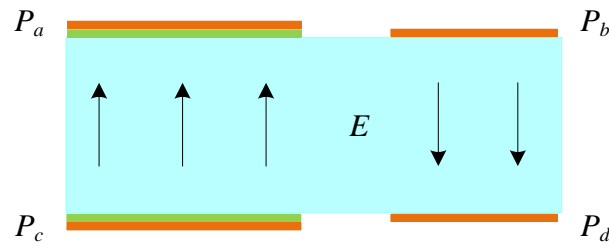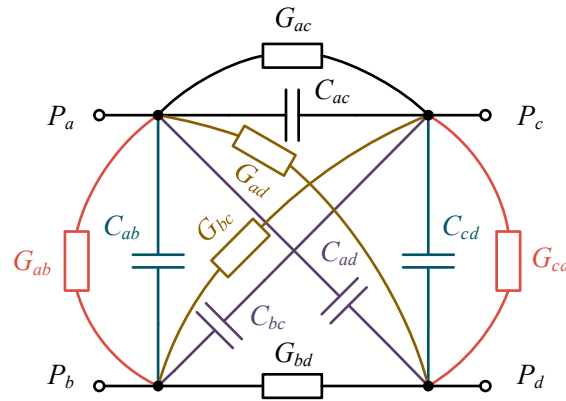
Figure 6. The novel underwater CPT coupler.

Figure 7. The equivalent circuit of the proposed CPT coupler.

As the transmission distance increases, the equivalent conductance decreases, resulting in a lower power transfer efficiency. To reduce power losses, metal plates P_a and P_c, as well as P_b and P_d, are kept in close proximity. In the envisioned practical application, the overall structure of the underwater CPT system is depicted in Figure 8, where the equivalent electrical conductance G_{bd} in Figure 7 approaches infinity. To simplify the analysis, this paper sets $C_{ad} = C_{bc}$, $G_{ad} = G_{bc}$, $C_{ab} = C_{cd}$, and $G_{ab} = G_{cd}$, with the conductance G_{bd} approaching infinity, as mentioned earlier.
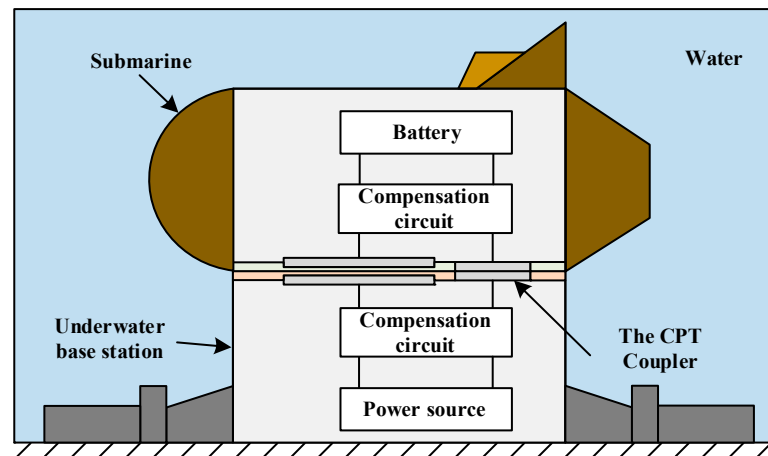

Figure 8. An underwater CPT system in practical application.

Therefore, the equivalent circuit shown in Figure 7 can be simplified to the circuit shown in Figure 9, where $G_{P1} = G_{ab} + G_{ad}$, $G_{S1} = G_{bc} + G_{cd}$, $G_{m1} = G_{ac}$, $C_{M1} = C_{ac}$, $C_{P1} = C_{ab} + C_{ad}$, and $C_{S1} = C_{bc} + C_{cd}$.
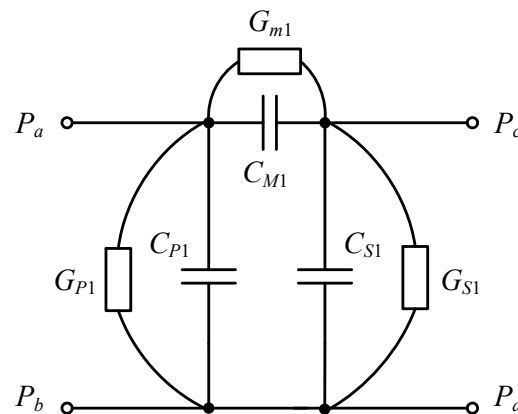
Figure 9. The simplified circuit of the proposed CPT coupler.

4.2. Analysis of the Underwater CPT System with a Double-Sided LC Compensation Circuit

A parallel model is used to represent the equivalent conductance and resistance between the underwater metal plates. In reality, the parameters between the metal plates do not follow a simple parallel relationship. Thus, the specific values of related parameters cannot be measured using an LCR analyzer. And it is necessary to build a CPT system to measure the equivalent parameters of the underwater CPT system.

Many high-performance compensation circuits have been proposed, such as the double-sided LC compensation circuit [12,29] and the double-sided LCLC compensation circuit [30,31]. The double-sided LC-compensated CPT circuit is selected to conduct experiments due to its advantages of simple construction and good filter capacity. As shown in Figure 10, the input inverter consists of four MOSFETs $Q_{1,2,3,4}$. The DC voltage U_{DC} is converted to a square-wave voltage v_{AB}. Since a higher order compensation circuit is applied, fundamental harmonic approximation (FHA) is used. For the underwater CPT system, it is necessary to choose an appropriate frequency f to achieve the input zero phase angle (ZPA). This helps eliminate most input reactive power and achieve a soft switching of MOSFETs.
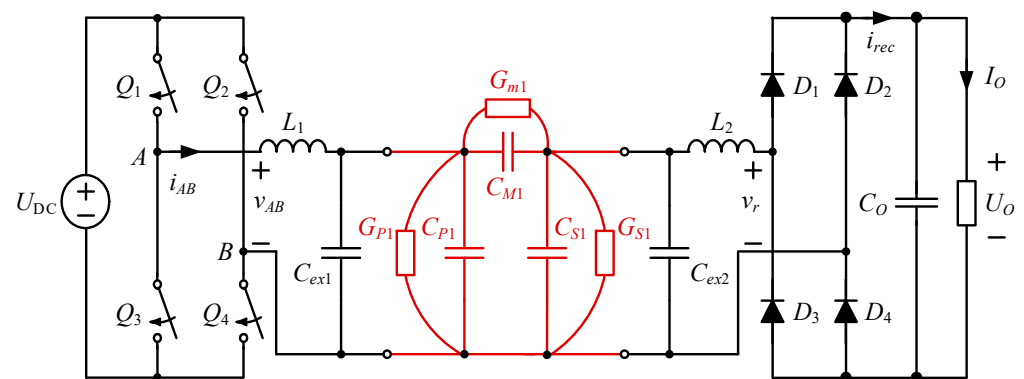

Figure 10. An underwater CPT circuit based on the double-sided LC compensation network.

To simplify the analysis, the CPT circuit shown in Figure 10 can be made equivalent to the circuit shown in Figure 11. The DC voltage source U_{DC} in Figure 10 generates a square wave voltage v_{AB} through the full-bridge inverter circuit, where the duty cycle of the full-bridge inverter circuit is represented as D. The v_{IN} shown in Figure 11 represents the fundamental component of v_{AB}, and it can be calculated as:

$$v_{\text{in}}(t) = \frac{4V_{IN}}{\pi} \sin \frac{\pi D}{2} \sin(\omega t + \theta). \tag{5}$$
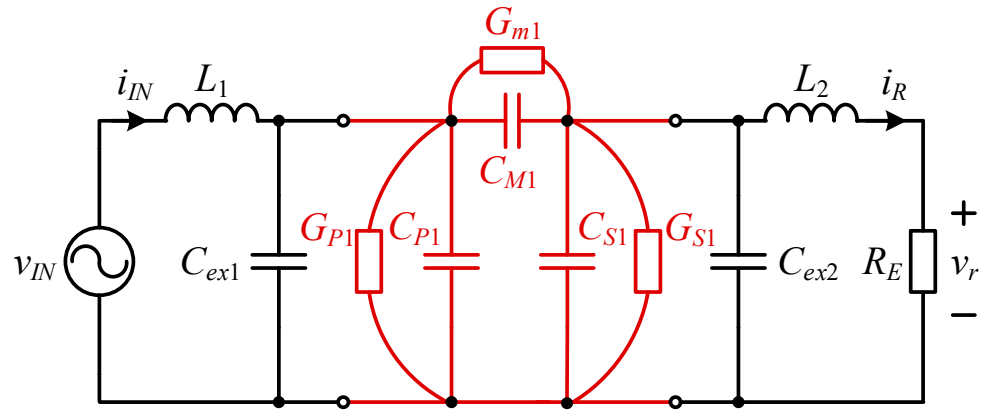
Figure 11. The simplified double-sided LC-compensated CPT circuit.

If the equivalent load is R_E, then $R_E = (8/\pi^2) R_L$. Defining $L_1 = L_2$, $C_{pri} = C_{ex1} + C_{P1}$, $C_{sec} = C_{ex2} + C_{S1}$, and $C_{ex1} = C_{ex2}$, the equivalent capacitors $C_{pri} = C_{sec}$. The expression of input impedance Z_{in} is given by

$$Z_{\text{in}} = j\omega L_1 + (\frac{1}{G_{P1}} + \frac{1}{j\omega C_{pri}}) || [\frac{1}{G_{m1}} || \frac{1}{j\omega C_M} + \frac{1}{G_{P1}} || \frac{1}{j\omega C_{pri}} || (R_E + j\omega L_1)]. \tag{6}$$

The expression for the input current i_{IN} is

$$i_{IN} = \frac{v_{IN}}{Z_{IN}}. \tag{7}$$

The expression for the output current i_R is

$$i_R = \frac{v_{IN} Z_1 (Z_L || Z_1)}{Z_L (Z_1 + Z_2 + Z_L || Z_1)[Z_L + Z_1 || (Z_2 + Z_L || Z_1)]}. \tag{8}$$

The expressions for Z_1, Z_2, and Z_L are defined as $Z_1 = 1/(j\varepsilon C_{pri} + G_{P1})$, $Z_2 = 1/(j\varepsilon C_{M1} + G_{m1})$, and $Z_L = 1/(j\varepsilon L_1)$.

The expression for the output voltage v_R is

$$v_R = i_R R_E. \tag{9}$$

After rectifying and filtering, the output voltage is given by

$$V_0 = \frac{\pi}{4} V_r. \tag{10}$$

According to Figure 8, the proposed CPT coupler exhibits symmetry between the primary and secondary sides. Therefore, for the proposed CPT coupler, there are four unknown parameters within the coupler, namely G_{m1}, C_{M1}, $G_{P1} = G_{S1}$, and $C_{P1} = C_{S1}$. Thus, it is necessary to establish four independent equations to solve for these four unknown parameters. A flow chart for solving the equivalent parameters of the proposed coupler is given in Figure 12.

Two different resistive loads, R_1 and R_2, are selected. Parameters U_{DC}, C_{ex1}, C_{ex2}, L_1, and L_2 are all predesigned. When the load is R_1, the operating frequency is adjusted until the input impedance becomes approximately resistive. Then, current operating frequency f_{R1}, input power $P(R_1)$, and output voltage $U_O(R_1)$ are all recorded. When the load is R_2, the operating frequency is adjusted until the input impedance becomes approximately resistive. Then, the current operating frequency f_{R2}, input power $P(R_2)$, and output voltage $U_O(R_2)$ are recorded. Substituting measured parameters f_{R1}, $P(R_1)$, f_{R2}, and $P(R_2)$ into (7) and (10), parameters G_{m1}, C_{M1}, G_{P1}, and C_{S1} of the proposed CPT coupler can be calculated.
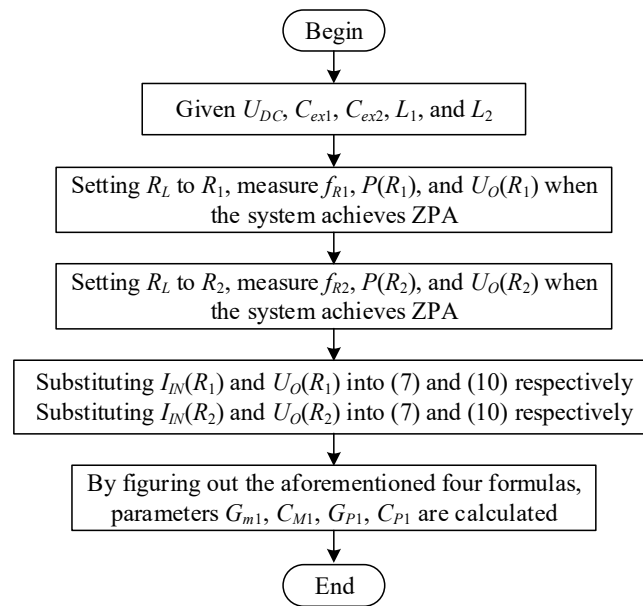
Figure 12. Flow chart for solving equivalent parameters of the proposed coupler.

To validate the calculated parameters, a new experiment using a third resistive load R_3 is carried out. The frequency f_{R3}, input power $P(R_3)$, output voltage $U_O(R_3)$, and the DC-to-DC efficiency are measured when the circuit achieves input ZPA. Calculate the theoretical efficiency of the double-sided LC-compensated CPT circuit. If the measured efficiency is approximately equal to the theoretical value, it proves that the calculated parameters G_{m1}, C_{M1}, G_{P1}, and C_{P1} are correct.

5. Experimental Validation

To validate the above analysis, an underwater double-sided LC-compensated CPT circuit was constructed based on the proposed underwater CPT coupler. The overall structure of the underwater CPT coupler in the experiment is shown in Figure 13. A water tank is used to simulate the underwater environment, with dimensions of approximately 50 cm in length, 40 cm in width, and 30 cm in height. Metal plates are made of aluminum, with only one pair of metal plates insulated. The dimensions of the metal plates are 200 mm × 200 mm × 2 mm. The insulating material used is PVC with a thickness of d_{PVC} = 4 mm. To prevent water seepage, the metal plates and insulation layers are sealed in airtight bags with a thickness of 200 microns. The dimensions of the other pair of metal plates are 100 mm × 100 mm × 2 mm. These two pairs of metal plates were fully immersed in the tap water without insulation.
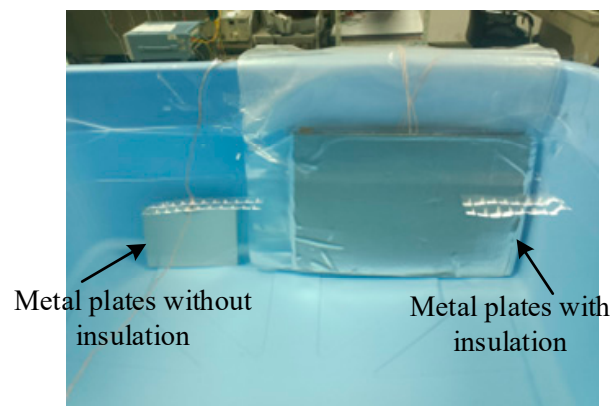

Figure 13. The structure of the proposed CPT coupler.

Microcontroller TMS320F28335 is used to drive $Q_{1,2,3,4}$. SiC MOSFETs IMW120R045M1 are selected to construct the inverter. SiC diodes IDW30G65C5 are adopted to realize rectification. The TMS320F28335 DSP has a high-speed processing capability of 150 MHz, up to six enhanced pulse width modulator (EPWM) modules, and an easy-to-implement PWM output control program. Therefore, the TMS320F28335 is suitable for generating high-frequency inverter drive signals [32]. The compensation capacitors C_{ex1} and C_{ex2} are set to 1 nF, while the compensation inductors L_1 and L_2 are set to 240 µH. Two loads, $R_1 = 50\ \Omega$ and $R_2 = 200\ \Omega$, are chosen in this experiment. All components except the CPT coupler are assumed to operate in ideal conditions with no parasitic parameters. Therefore, any losses observed during the experiment are solely attributed to the coupler.

Experimental waveforms are shown in Figure 14, where v_{GS} is the drive voltage of the switching devices, v_{AB} is the high-frequency input voltage, i_{IN} is the input current, and U_O is the output voltage. According to Figure 14, for different loads R_1 and R_2, the input currents are nearly in phase with the input voltages, respectively. This indicates that the input ZPA are all realized.
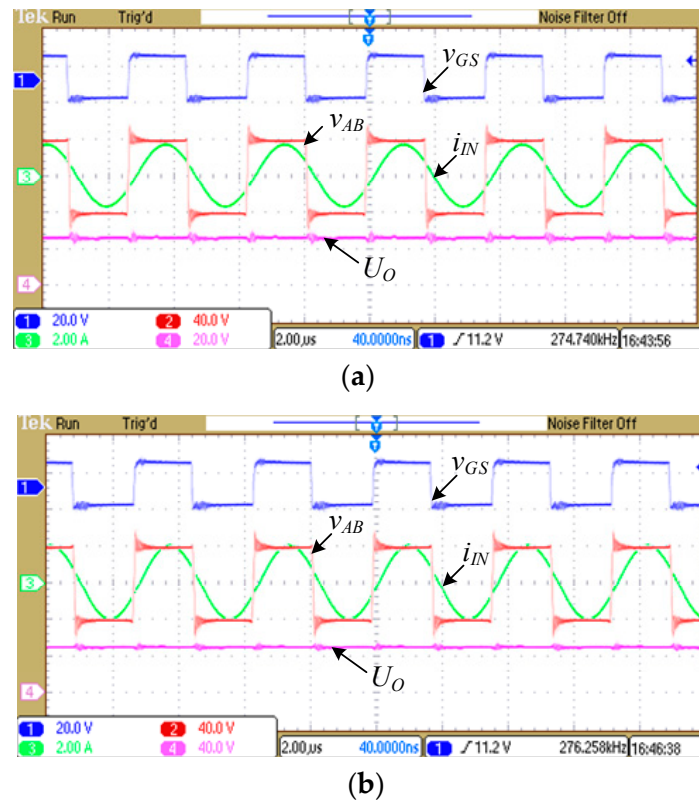

(**a**)

(**b**)

Figure 14. Experiment waveforms of the underwater CPT circuit. (**a**) $R_1 = 50\ \Omega$; (**b**) $R_2 = 200\ \Omega$.

Experimental parameters of the double-sided LC-compensated CPT circuit with different loads are shown in Table 5. Since the tap water is conductive and the equivalent resistor of the tap water is quite large, a significant amount of output power is wasted, resulting in reduced efficiency compared to the air. As a result, the analysis conducted for the double-sided LC-compensated CPT circuit in the air is not applicable to underwater CPT systems.

Table 5. Measured parameters of the double-sided LC-compensated CPT circuit in tap water.

R_L	f	P_{IN}	U_{DC}	U_O	η
50 Ω	274.7 kHz	38.8 W	40 V	26 V	34.85%
200 Ω	276.3 kHz	47.78 W	40 V	48 V	24.11%

The efficiency η shown in Table 5 represents the measured efficiency from the DC source to the DC load. Although the efficiency of the underwater CPT circuit with the proposed coupler is still relatively low, there has been an improvement in both power transfer level and efficiency compared to previous related research. Following the design process shown in Figure 12, when $R_1 = 50\ \Omega$, parameters P_{IN}, U_{DC}, and U_O in Table 5 are substituted into (7) and (10). Similarly, when $R_2 = 200\ \Omega$, parameters P_{IN}, U_{DC}, and U_O in Table 5 are substituted into (7) and (10). With the aforementioned four equations, the equivalent parameters of the proposed coupler can be derived. Relevant parameters are given in Table 6.

Table 6. Equivalent capacitances and conductance of the underwater coupler.

G_{m1}	$G_{P1} = G_{S1}$	C_{M1}	$C_{P1} = C_{S1}$
1.786×10^{-5} S/m	7.194×10^{-5} S/m	105 pF	251 pF

To validate the aforementioned parameter calculation procedure, a verification experiment is conducted with $R_3 = 10\ \Omega$. The experimental waveform is shown in Figure 15. The operating frequency f_3 is 274.76 kHz, and the input voltage and input current are nearly in phase, which indicates that nearly all input ZPA and soft-switching of MOSFETs are achieved. The measured input power and DC-DC efficiency with $R_3 = 10\ \Omega$ are 39.89 W and 19%, respectively. With the equivalent parameters of the proposed coupler shown in Table 6, the theoretical efficiency for load $R_3 = 10\ \Omega$ is calculated to be 22.2%. The measured efficiency closely matches the theoretical calculation, demonstrating the correctness of the parameter calculation procedure. The gap between the measured efficiency and the theoretical efficiency is caused by parasitic parameters in the inverter circuit, compensation network, and rectifier circuit.
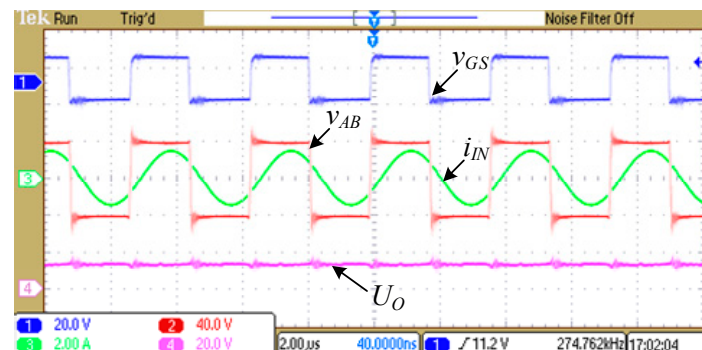

Figure 15. Waveforms of v_{GS}, v_{AB}, i_{IN}, and I_O when $R_3 = 10\ \Omega$.

According to the experimental analysis, the innovative points of this paper are mainly reflected in two aspects. Firstly, the proposed underwater coupler and the parameter design procedure function effectively. According to Figures 14 and 15, it can be observed that the proposed underwater CPT system is capable of achieving both input ZPA and predesigned output power. Secondly, there is an improvement in both the output power and efficiency of the underwater CPT system. The operating frequency, output power, and efficiency of the proposed coupler submerged in tap water are given in Table 7. Compared to previous research given in Table 1, the proposed underwater system is more suitable for practical implementation.

For a better comparison with other studies, Table 7 summarizes the coupler structure, transmission power, and transmission efficiency of the proposed underwater CPT system. The output power and efficiency of the proposed CPT system are still relatively low. However, compared to [25], shown in Table 1, the proposed CPT system can operate in natural water environments. Compared to [4,26,28], since the operating frequency is 275 kHz, the proposed CPT system can operate within the most frequently utilized

frequency range. Compared to [27], the transferred power and efficiency are all improved. In addition, as mentioned in the Introduction, in [4,26–28], only a small amount of water is added between the metal plates of the CPT coupler. Clearly, when the metal plates are fully immersed in a larger water tank, the system's efficiency would significantly decrease.

Table 7. The coupler structure, transmission power, and transmission efficiency of the proposed coupler.

Insulation	Water Types	Transfer Distance	Input Power	Efficiency
Only one pair of plates is insulated	Tap water	8 mm	38.8 W	34.85% ($R = 50\ \Omega$)

Based on the newly designed coupler in this paper, with a working frequency of 275 kHz, it achieves several tens of watts of power transmission in tap water. Without efficiency optimization, the maximum efficiency is 34.85%. Therefore, compared to existing research, the underwater CPT coupler designed in this paper not only reduces design complexity but also enhances the performance of the CPT system in tap water. However, in-depth research is still needed to further improve the efficiency of underwater CPT systems.

6. Conclusions

This paper analyses the single pair and two pairs of metal plates in different media with varying electrical conductivity. Since natural water is conductive, the traditional CPT coupler used in air cannot realize power transfer in water. Thus, after a comprehensive analysis of underwater CPT couplers, a novel CPT coupler is proposed to improve the power transfer level and efficiency of underwater CPT systems. To calculate the equivalent capacitances and conductance of the novel CPT coupler, a double-sided LC-compensated CPT circuit with the proposed CPT coupler submerged in tap water is built. The operating frequency is 275 kHz, efficiency is 34.85%, and the input power is 38.8 W. Through experimental validation, it is demonstrated that compared to traditional underwater CPT systems, the power transfer level and efficiency of the double-sided LC-compensated CPT circuit are improved, expanding the applicability of CPT technology. However, unlike IPT, which has been developed for a long time, researches of CPT technology in both air and water mediums have only been carried out very recently. In order to put CPT systems into practice as soon as possible, it is important to work out the operating principle of the underwater CPT and enhance the power transfer distance, power transfer level, and efficiency of the whole system.

Author Contributions: Methodology, X.Z.; validation, J.L.; writing—original draft, X.Z.; supervision, J.L. All authors have read and agreed to the published version of the manuscript.

Data Availability Statement: Data are contained within the article.

Conflicts of Interest: The authors declare no conflict of interest.

References

1. Bogue, R. Underwater robots: A review of technologies and applications. *Ind. Robot. Int. J.* **2015**, *42*, 186–191. [CrossRef]
2. Sahoo, A.; Dwivedy, S.K.; Robi, P. Advancements in the field of autonomous underwater vehicle. *Ocean Eng.* **2019**, *181*, 145–160. [CrossRef]
3. Rong, E.; Sun, P.; Zhang, X.; Yang, G.; Wu, X. 3.3 kW Underwater Capacitive Power Transfer System for Electric Ship Charging Application. In Proceedings of the 2023 IEEE International Conference on Power Science and Technology (ICPST), Kunming, China, 5–7 May 2023; pp. 1052–1057.
4. Tamura, M.; Naka, Y.; Murai, K.; Nakata, T. Design of a capacitive wireless power transfer system for operation in fresh water. *IEEE Trans. Microw. Theory Tech.* **2018**, *66*, 5873–5884. [CrossRef]
5. Hayslett, T.M.; Orekan, T.; Zhang, P. Underwater wireless power transfer for ocean system applications. In Proceedings of the OCEANS 2016 MTS/IEEE Monterey, Monterey, CA, USA, 19–23 September 2016; IEEE: Toulouse, France, 2016; pp. 1–6.

6. Yang, L.; Li, X.; Zhang, Y.; Feng, B.; Yang, T.; Wen, H.; Tian, J.; Zhu, D.; Huang, J.; Zhang, A.; et al. A review of underwater inductive wireless power transfer system. *IET Power Electron.* **2023**. [CrossRef]

7. Sun, P.; Wu, X.; Cai, J.; Wang, X.; Zhang, X.; Liang, Y.; Xiong, Q.; Rong, E. Eddy current loss analysis and frequency optimization design of double-sided LCC-IPT system in seawater environment. *Sci. China Technol. Sci.* **2022**, *65*, 407–418. [CrossRef]

8. Kim, J.; Kim, H.; Kim, D.; Park, J.; Park, B.; Huh, S.; Ahn, S. Analysis of eddy current loss for wireless power transfer in conductive medium using Z-parameters method. In Proceedings of the 2020 IEEE Wireless Power Transfer Conference (WPTC), Piscataway, NJ, USA, 15–19 November 2020; IEEE: Toulouse, France, 2020; pp. 432–434.

9. Mahdi, H.; Hoff, B.; Østrem, T. Optimal solutions for underwater capacitive power transfer. *Sensors* **2021**, *21*, 8233. [CrossRef]

10. Zhang, H.; Lu, F.; Hofmann, H.; Liu, W.; Mi, C.C. A four-plate compact capacitive coupler design and LCL-compensated topology for capacitive power transfer in electric vehicle charging application. *IEEE Trans. Power Electron.* **2016**, *31*, 8541–8551.

11. Lu, F.; Zhang, H.; Mi, C. A two-plate capacitive wireless power transfer system for electric vehicle charging applications. *IEEE Trans. Power Electron.* **2017**, *33*, 964–969. [CrossRef]

12. Lu, F.; Zhang, H.; Hofmann, H.; Mi, C.C. A double-sided LC-compensation circuit for loosely coupled capacitive power transfer. *IEEE Trans. Power Electron.* **2017**, *33*, 1633–1643. [CrossRef]

13. Naka, Y.; Tamura, M. Design of a capacitive coupler for underwater wireless power transfer focused on the landing direction of a drone. *IEICE Trans. Electron.* **2023**, 2023ECP5023. [CrossRef]

14. Tamura, M.; Murai, K.; Matsumoto, M. Design of conductive coupler for underwater wireless power and data transfer. *IEEE Trans. Microw. Theory Tech.* **2020**, *69*, 1161–1175. [CrossRef]

15. Yang, L.; Ju, M.; Zhang, B. Bidirectional undersea capacitive wireless power transfer system. *IEEE Access* **2019**, *7*, 121046–121054. [CrossRef]

16. Zhang, H.; Lu, F. Feasibility study of the high-power underwater capacitive wireless power transfer for the electric ship charging application. In Proceedings of the 2019 IEEE Electric Ship Technologies Symposium (ESTS), Washington, DC, USA, 14–16 August 2019; pp. 231–235.

17. Lu, F.; Zhang, H.; Mi, C. A review on the recent development of capacitive wireless power transfer technology. *Energies* **2017**, *10*, 1752. [CrossRef]

18. Abramov, E.; Alonso, J.M.; Peretz, M.M. Analysis and behavioural modelling of matching networks for resonant-operating capacitive wireless power transfer. *IET Power Electron.* **2019**, *12*, 2615–2625. [CrossRef]

19. Sinha, S.; Kumar, A.; Regensburger, B.; Afridi, K.K. A new design approach to mitigating the effect of parasitics in capacitive wireless power transfer systems for electric vehicle charging. *IEEE Trans. Transp. Electrif.* **2019**, *5*, 1040–1059. [CrossRef]

20. Ageev, I.; Rybin, Y.M. Features of Measuring the Electrical Conductivity of Distilled Water in Contact with Air. *Meas. Tech.* **2020**, *62*, 923–927. [CrossRef]

21. Pawlowicz, R. Calculating the conductivity of natural waters. *Limnol. Oceanogr. Methods* **2008**, *6*, 489–501. [CrossRef]

22. Pryor, R.W. Inductive conductivity measurement of seawater. In Proceedings of the COMSOL Conference, Rotterdam, The Netherlands, 23–25 October 2013.

23. Huang, L.; Hu, A.P. Defining the mutual coupling of capacitive power transfer for wireless power transfer. *Electron. Lett.* **2015**, *51*, 1806–1807. [CrossRef]

24. Mahdi, H.; Hoff, B.; Østrem, T. Maximum available efficiency of undersea capacitive coupling in a wireless power transfer system. In Proceedings of the 2021 IEEE 30th International Symposium on Industrial Electronics (ISIE), Kyoto, Japan, 20–23 June 2021; IEEE: Piscataway, NJ, USA, 2021; pp. 1–5.

25. Zhang, H.; Lu, F. Insulated coupler structure design for the long-distance freshwater capacitive power transfer. *IEEE Trans. Ind. Inform.* **2019**, *16*, 5191–5201. [CrossRef]

26. Tamura, M.; Murai, K.; Naka, Y. Capacitive coupler utilizing electric double layer for wireless power transfer under seawater. In Proceedings of the 2019 IEEE MTT-S International Microwave Symposium (IMS), Boston, MA, USA, 2–7 June 2019; IEEE: Piscataway, NJ, USA, 2019; pp. 1415–1418.

27. Urano, M.; Ata, K.; Takahashi, A. Study on underwater wireless power transfer via electric coupling with a submerged electrode. In Proceedings of the 2017 IEEE International Meeting for Future of Electron Devices, Kansai (IMFEDK), Kyoto, Japan, 29–30 June 2017; IEEE: Piscataway, NJ, USA, 2017; pp. 36–37.

28. Tamura, M.; Naka, Y.; Murai, K. Design of capacitive coupler for wireless power transfer under fresh water focusing on kQ product. In Proceedings of the 2018 IEEE/MTT-S International Microwave Symposium-IMS, Philadelphia, PA, USA, 10–15 June 2018; IEEE: Piscataway, NJ, USA, 2018; pp. 1257–1260.

29. Yi, L.; Moon, J. Design of efficient double-sided LC matching networks for capacitive wireless power transfer system. In Proceedings of the 2021 IEEE PELS Workshop on Emerging Technologies: Wireless Power Transfer (WoW), San Diego, CA, USA, 1–4 June 2021; IEEE: Piscataway, NJ, USA, 2021; pp. 1–5.

30. Lu, F.; Zhang, H.; Hofmann, H.; Mi, C.C. A Double-Sided LCLC-Compensated Capacitive Power Transfer System for Electric Vehicle Charging. *IEEE Trans. Power Electron.* **2015**, *30*, 6011–6014. [CrossRef]

31. Gao, F.; Wang, Z.; Li, L.; Wang, S.; Deng, J. Analysis and design of double-sided LCLC compensation parameters with coupling-insensitive ZVS operation for capacitive power transfer. In Proceedings of the 2019 IEEE Energy Conversion Congress and Exposition (ECCE), Baltimore, MD, USA, 29 September–3 October 2019; IEEE: Piscataway, NJ, USA, 2019; pp. 576–581.
32. Pang, S.; Xu, J.; Li, H.; Ma, Q.; Li, X. Dual-Frequency Modulation to Achieve Power Independent Regulation for Dual-Load Underwater Wireless Power Connector. *IEEE J. Emerg. Sel. Top. Power Electron.* **2022**, *11*, 2377–2389. [CrossRef]